RESEARCH PAPER

RNA Biology 10:6, 1017–1029; June 2013; © 2013 Landes Bioscience

Genome-wide identification of translationally inhibited and degraded miR-155 targets using RNA-interacting protein-IP

Jan Meier, Volker Hovestadt, Marc Zapatka, Armin Pscherer,† Peter Lichter* and Martina Seiffert

German Cancer Research Center; Division of Molecular Genetics; Heidelberg, Germany

†Current address: BioRN cluster management GmbH; Heidelberg, Germany

Keywords: RIP-Seq, AGO2-IP, miR-155, translational inhibition, miRNA target profiling, miRNA activity

Abbreviations: miRNA, microRNA; IP, immuneprecipitate; TL, total lysate; RIP, RNA-interacting protein immune precipitation; Seq, high-throughput sequencing; qPCR, quantitative real-time PCR; RISC, RNA-induced silencing complex; STDEV, standard deviation; SILAC, stable isotope labeling of amino acids in cell culture

MicroRNAs (miRNAs) are single-stranded, small, non-coding RNAs, which fine-tune protein expression by degrading and/or translationally inhibiting mRNAs. Manipulation of miRNA expression in animal models frequently results in severe phenotypes indicating their relevance in controlling cellular functions, most likely by interacting with multiple targets. To better understand the effect of miRNA activities, genome-wide analysis of their targets are required. MicroRNA profiling as well as transcriptome analysis upon enforced miRNA expression were frequently used to investigate their relevance. However, these approaches often fail to identify relevant miRNAs targets. Therefore, we tested the precision of RNA-interacting protein immunoprecipitation (RIP) using AGO2-specific antibodies, a core component of the "RNA-induced silencing complex" (RISC), followed by RNA sequencing (Seq) in a defined cellular system, the HEK293T cells with stable, ectopic expression of miR-155. Thereby, we identified 100 AGO2-associated mRNAs in miR-155-expressing cells, of which 67 were in silico predicted miR-155 target genes. An integrated analysis of the corresponding expression profiles indicated that these targets were either regulated by mRNA decay or by translational repression. Of the identified miR-155 targets, 17 were related to cell cycle control, suggesting their involvement in the observed increase in cell proliferation of HEK293T cells upon miR-155 expression. Additional, secondary changes within the gene expression profile were detected and might contribute to this phenotype as well. Interestingly, by analyzing RIP-Seq data of HEK-293T cells and two B-cell lines we identified a recurrent disproportional enrichment of several miRNAs, including miR-155 and miRNAs of the miR-17-92 cluster, in the AGO2-associated precipitates, suggesting discrepancies in miRNA expression and activity.

Introduction

MicroRNAs (miRNAs) bind to their target mRNAs via a 6–8 nt seed sequence located in the 5' part of the mature miRNA.[1] Once a specific mRNA is attached to a miRNA within the "RNA-induced silencing complex" (RISC), the translation of the mRNA is inhibited and/or the mRNA is degraded. To what extent mRNA targets are either cleaved or merely translationally inhibited is still a matter of debate.[2-7] Genetic mouse models with manipulated miRNA expression levels frequently show severe phenotypes. For instance, mice lacking miR-155 show impaired immune responses, whereas mice overexpressing miR-155 exhibit perturbed peripheral blood cell populations.[8,9] As miRNAs are known as fine-tuners of gene expression and often have only limited impact on single targets, the interaction of a single miRNA with a single target mRNA might not easily explain the pronounced phenotypes. To identify miRNA-mRNA interactions and their relevance for phenotypic changes, overexpression of miRNAs followed by transcriptome analyses were frequently used. This approach has however several weaknesses. First, effects on primary miRNA targets cannot be distinguished from indirect or secondary effects on gene expression. Second, miRNA targets that are regulated by translational repression are missed by this approach. Even though miRNA expression profiling is commonly used to characterize their role in diseases like cancer, it is not clear whether these profiles reflect the actual activity of miRNAs. To investigate this question and to identify miRNA targets in a genome-wide approach, we used RNA-interacting protein IP followed by next-generation sequencing of co-precipitated RNAs (RIP-Seq)[10-14] using HEK293T cells with ectopic miR-155 expression, as a defined isogenic cell model. This approach allowed us to test the precision of the RIP-Seq

*Correspondence to: Peter Lichter; Email: peter.lichter@dkfz.de
Submitted: 01/04/13; Revised: 04/03/13; Accepted: 04/04/13
http://dx.doi.org/10.4161/rna.24553

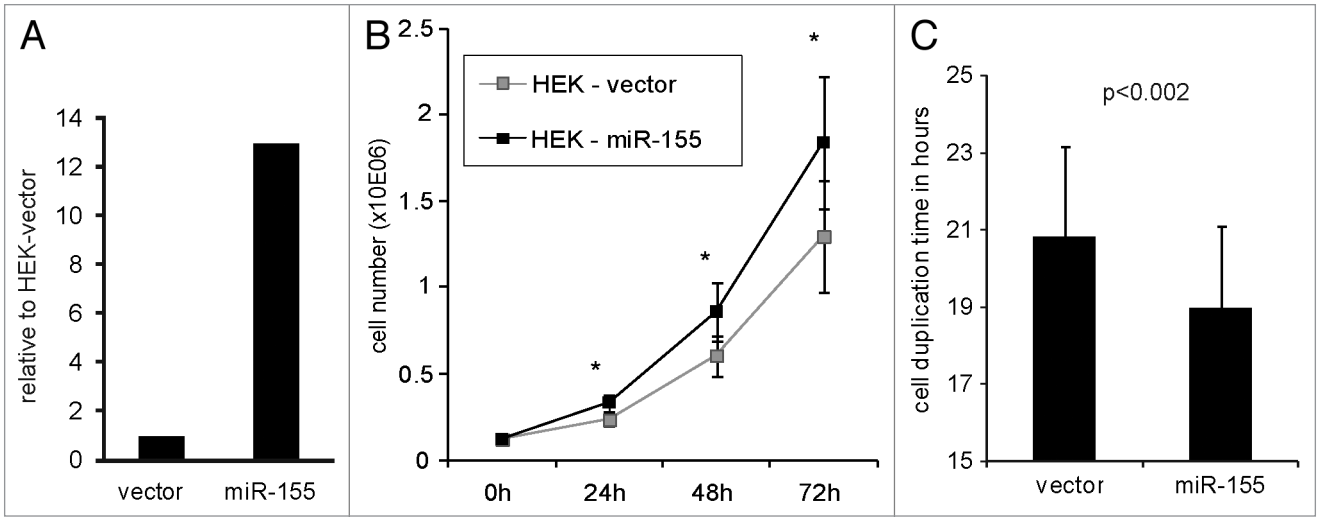

Figure 1. Proliferation of HEK-vector and HEK-miR-155 cells. (**A**) Quantification of miR-155 expression in HEK-vector and HEK-miR-155 cells by qPCR. The miR-155 levels were normalized to the expression of the housekeeping small RNA RNU-6B. (**B**) HEK-vector and HEK-miR-155 cells were seeded at 3 x 10^5 (1.2 x 10^5/ml) cells per well in 6-well culture plates and viable cells were quantified after 24 h (n = 7), 48 h (n = 9) and 72 h (n = 8) using a Vicell Counter. Statistical significance was calculated using student's t-test (* $p < 0.05$). (**C**) Average cell doubling-times over 72 h were calculated ($p < 0.002$). The indicated error-bars represent standard deviations.

method and to identify functionally related miR-155 targets. By integrating AGO2-IP profiles and corresponding gene expression profiles, which were generated by RIP-Seq, we wanted to dissect secondary changes of the expression profile, which might be induced by the enforced miR-155 expression. We further aimed at testing whether and to what extent miRNA targets are regulated by mRNA decay or translational inhibition.

Results

Ectopic miR-155 expression results in increased proliferation of HEK293T cells. In order to test the accuracy of the RIP-Seq method, (1) to identify functionally relevant miRNA targets, (2) to delineate the secondary consequences of ectopic miRNA expression and (3) to determine the actual mode of miRNA activity, we stably transfected HEK293T cells that have a low endogenous miR-155 expression, with a miR-155 expression vector to generate a HEK-miR-155 cell line. After culturing cells under selective conditions for up to 3 mo, miR-155 levels were analyzed at three different time points by quantitative real-time PCR (qPCR), which revealed a miR-155 overexpression between 13- and 28-fold relative to the control cell line carrying the vector backbone (HEK-vector). The HEK-miR-155 cells that were used for the RIP-Seq experiments showed a 13-fold overexpression of miR-155 (**Fig. 1A**). To study the impact of miR-155 on the phenotype, we compared cell viability and proliferation rates of HEK-miR-155 cells with the control cell line. Cell counts and viabilities were determined 24, 48 and 72 h after seeding equal amounts of cells. Seven independent experiments were performed over a period of more than 3 mo. HEK-miR-155 cells had a significantly higher proliferation rate compared with HEK-vector cells with on average 30% more cells after 72 h of culture (**Fig. 1B**). Cell duplication times within the first 72 h of cultivation of HEK-vector and HEK-miR-155 cells were calculated and were 20.8 and 19 h, respectively (**Fig. 1C**). No significant differences in cell viability between both cell lines were observed. To further validate these findings, we performed EdU incorporation assays detecting DNA replication rates as an indicator for proliferation. Synchronized cells were cultured for 6 h in the presence of EdU and cells with active replication were quantified by flow cytometry, which revealed a 7% increase in proliferation of HEK-miR-155 cells (**Fig. S1**).

Extensive changes in mRNA profiles induced by ectopic miR-155 expression. In order to identify changes in the miRNome and targetome upon ectopic miR-155 expression, RIP-Seq experiments using HEK-miR-155 and HEK-vector cells were performed. In addition, mRNA-Seq of the total lysates of both cell lines was performed to dissect changes on the cellular gene expression profile, which were directly and indirectly caused by the enforced expression of miR-155. The specificity of AGO2 immunoprecipitation was confirmed by western blot analyses (**Fig. S2**) and mass spectrometry. For quality control, we tested the enrichment of miR-155 in the AGO2 IPs by qPCR. As expected, miR-155 was almost absent in the IP fractions of HEK-vector cells, but specifically enriched in the AGO2 IP of HEK-miR-155 cells with a more than 7-fold enrichment compared with the control IP with isotype antibodies (**Fig. S3**).

The mRNA content of the total lysate (TL) and immunoprecipitate (IP) fractions of three independently performed RIP experiments was analyzed by high-throughput sequencing. The obtained reads were mapped against the human reference genome version 19 using the TopHat algorithm.[15] For the IP and TL fractions on average 35M and 68M reads were generated, respectively. Comparing the mRNA profiles in the TL fractions of HEK-vector and HEK-miR-155 cells revealed that 339 mRNAs were downregulated and 121 mRNAs were

upregulated in HEK293T cells upon ectopic miR-155 expression (**Fig. 2A**, **Table 1**; **Table S1**). Notably, among the top 20 upregulated genes, we identified *CCND1* and all three members of the ETS transcription factor subfamily *PEA3,* which are *ETV1*, *ETV4* and *ETV5* (**Table S1**). Upregulation of these genes was confirmed by quantitative real-time PCR (**Fig. S4**). The IP fractions of both cell lines were compared, to identify transcripts enriched in the RISC. Here, 213 mRNAs with higher abundance and 409 mRNAs with lower abundance in the IP fraction of HEK-miR-155 cells were identified (**Fig. 2B**, **Table 1**; **Table S2**). Taken together, these data suggest that the enforced expression of miR-155 led to wide-spread secondary changes within the gene expression profile. Furthermore, these changes might subsequently have an impact on the IP profiles. For instance, *CCND1* was—besides being one of the most highly upregulated transcripts in HEK-miR-155—among the mRNAs, which were highly enriched in the IP of these cells. Computational miRNA target prediction for the *CCND1* 3'UTR indicated a potential miR-155 binding site and the presence of several miRNA target sites for miR-17, miR-19a, miR-15, miR-16-1, miR-20a and miR-106a, which were shown to be functionally active.[16,17] The miR-155 target gene *CEBPB*[18] was described to repress the expression of CCND1 in macrophages.[19] Furthermore, screening of the *CCND1* promotor region for protein interaction sites using the TFSEARCH algorithm revealed several putative CEBPB binding sites. We therefore performed knockdown experiments using *CEBPB*-specific siRNAs. Quantitative RT-PCR analysis revealed a knockdown of the *CEBPB* transcript of approximately 40% 24 h and 48 h after transfection. Associated with that, a slight increase of up to 1.8-fold of *CCND1* mRNA was observed (**Fig. S5**), suggesting that the increased expression of *CCND1* in HEK-miR-155 cells might be in part caused by miR-155-mediated downregulation of *CEBPB.* Therefore, its enrichment in the IP fraction might not be due to a direct interaction with miR-155, but rather reflects the higher abundance of this mRNA in the lysate of HEK-miR-155 cells and its subsequent interaction with endogenous miRNAs like miR-17 or miR-106a. Thus, in order to reliably identify miR-155 targets, mRNA levels detected in the IP fractions have to be normalized to their expression levels measured in the total lysates of the respective sample.

Identification of potential miR-155 target genes by RIP-Seq. The mRNA levels detected in the IP fractions were normalized to their respective TL fractions in order to compensate for changes in mRNA expression as described above. Therefore, log2-ratios of IP vs. TL values were calculated for each transcript and statistically significant differences between HEK-miR-155 and HEK-vector cells were obtained by performing a Significance Analysis of Microarrays (SAM). As a result, 100 transcripts were identified with significant enrichment in the IPs of HEK-miR-155 cells in comparison to the control cell line (false discovery rate 10%, SAM) (**Fig. 2C**, black, **Table 1**; **Table S3**). Notably, no significant enrichment of transcripts was observed in HEK-vector IPs (**Fig. 2C**). Prediction algorithms were used in order to identify putative miR-155 targets within the lists of co-precipitated mRNAs for the isogenic cell lines. For this purpose, five target prediction tools TargetScan, MiRANDA, DianaMicro-T, MiRWALK and PITA were used.[20-25] Transcripts predicted by at least three of these five algorithms with a seed match of seven or eight nucleotides and a p value lower than 0.05 were considered as putative miRNA targets predicting regulation of 67 (of 100) enriched mRNAs in HEK-miR-155 IPs (**Table 2**). At least 21 of these are experimentally validated miR-155 targets (**Table 2**; indicated with *).

To confirm an enrichment of target genes, qPCR was performed for the known miR-155 target *PHC2* in one technical and two biological replicates. Since *GAPDH* mRNA was not enriched in our RIP-Seq experiments, it was used as a negative control. The obtained results verified a consistent enrichment of *PHC2* mRNA in HEK-miR-155 IPs relative to HEK-vector IPs in all three experiments (data not shown). In accordance with the RNA-Seq data, *GAPDH* mRNA showed no consistent enrichment in HEK-miR-155 IPs, indicating specific precipitation of miR-155 targets. To identify functionally relevant transcripts regulated by miR-155, we searched the Ingenuity database for genes related to proliferation. Of the 100 genes enriched in HEK-miR-155 IPs, 25 were associated to proliferation and 17 of these were predicted as direct miR-155 targets (**Table 2**; bold letters). Notably, at least seven of these genes, among them *CEBPB*, *PHC2* and *TCF4*, were experimentally verified miR-155 targets.[18,26,27] By screening RIP-Seq data of two B-cell lines, MEC-1 and JEKO-1 (unpublished data), we observed an enrichment of 36 and 19 of the 67 putative HEK miR-155 targets in the respective IPs. We further tested *ZFP36*, *JARID2* and *BACH1* regulation after 24 h of anti-miR-155 treatment in MEC-1 cells by qRT-PCR. Accordingly, we observed a tendency of de-repression for all candidates, which was significant for *ZFP36*, a so far unknown miR-155 target (**Fig. S6**).

Degradation vs. translational repression of miR-155 targets. The modes of miRNA activity are still under debate. Recent data suggest that translational repression precedes mRNA deadenylation and decay.[3,28,29] Here, we investigated miRNA targets at a steady-state level to determine to which extent the identified miR-155 targets were degraded or translationally repressed. We therefore evaluated the expression levels of the 67 putative HEK miR-155 targets to identify transcripts with differential expression between HEK-vector and HEK-miR-155 cells. Out of these, nine targets (e.g., *BACH1* and *JARID2*) showed significantly lower levels of mRNA in the TL fraction, which might be explained by miR-155-mediated decay of the transcripts, but only a minor enrichment in the IP of HEK-miR-155 cells ($p < 0.05$). Furthermore, 20 targets showed a significant enrichment in the IP fraction ($p < 0.05$) but no significant change in the TL (e.g., *PHC2* and *DUSP14*), suggesting that these transcripts were primarily regulated by translational repression. One single target gene, *ZFP36*, was identified by a significant enrichment in the IP and a robust decay in the TL of HEK-miR-155 cells. To validate these findings, the expression levels of eight putative miR-155 targets were quantified by qRT-PCR using the TL fractions of HEK-vector and HEK-miR-155 cells. Thereby, we observed reduced mRNA levels for *ZFP36*, *ZNF652* and *BACH1* in HEK-miR-155 cells, whereas the mRNA levels of *PHC2*, *FBXO9*,

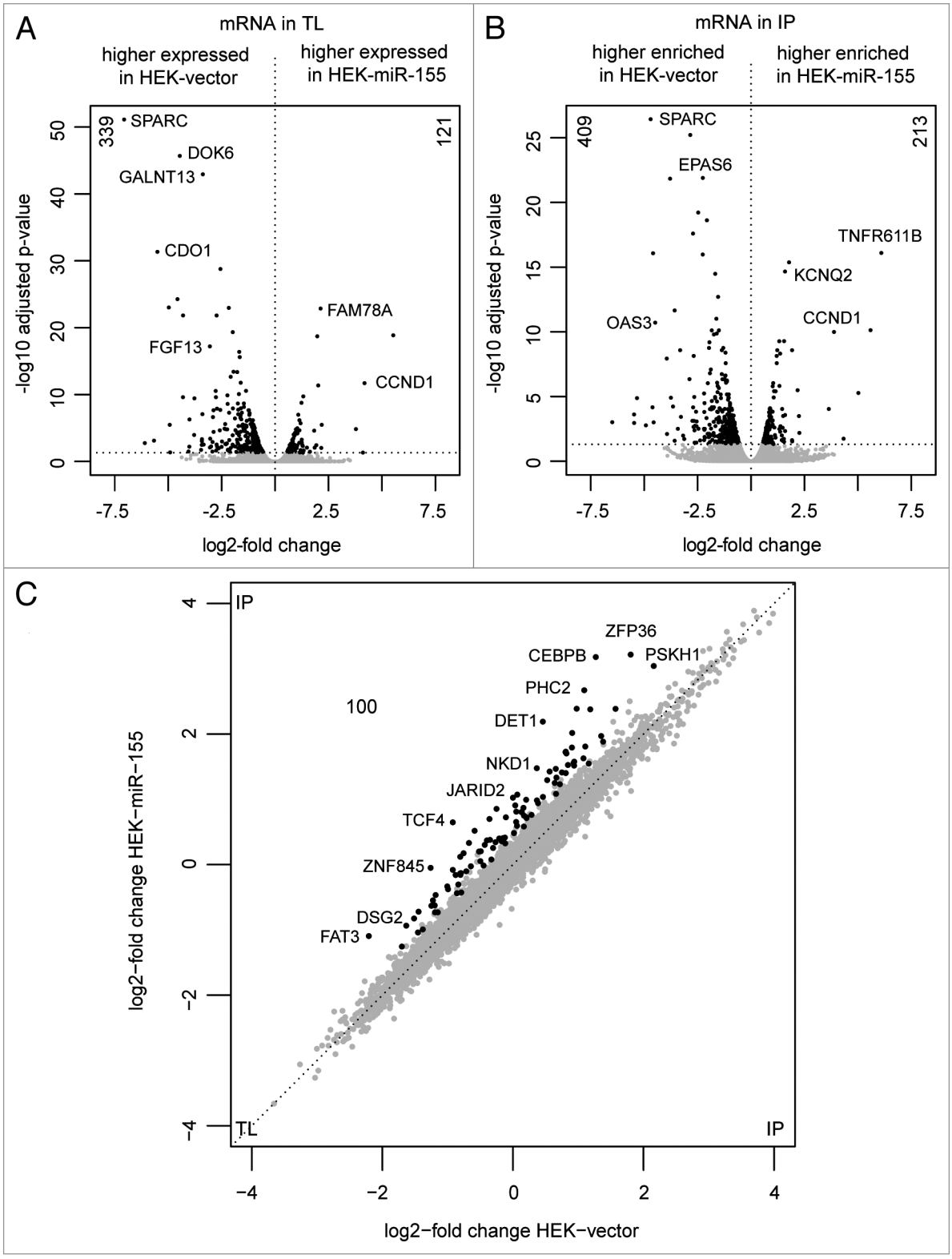

Figure 2. Volcano and starburst plots displaying significantly altered mRNAs within IP and TL fractions. Co-immunoprecipitated mRNAs of TL and IP fractions of three RIP experiments using HEK-vector and HEK-miR-155 cells were identified and quantified by next generation sequencing. (**A**) TL fractions of HEK-vector and HEK-miR-155 cells were compared. In total, 460 mRNAs showed differential expression between both cell lines, with 339 significantly downregulated and 121 significantly upregulated transcripts upon ectopic miR-155 expression ($p < 0.05$, black). (**B**) Comparing the IP fractions of both cell lines revealed 409 mRNAs with significantly lower levels and 213 mRNAs with significantly higher levels in HEK-miR-155 IPs ($p < 0.05$, black). (**C**) Transcripts with enhanced enrichment in the HEK-miR-155 IPs after compensation for secondary effects, like *TCF4, JARID2, PHC2 CEBPB* and *PHC2*, are displayed in black (FDR 10%, SAM).

AGTRAP and *DUSP14* were similar in both isogenic cell lines (**Fig. 3A**), confirming the RNA sequencing data.

To test for the regulation of identified miR-155 target genes on protein level, 3'UTR luciferase sensor assays were performed for *CEBBP*, *PHC2*, *DUSP14* and *MAP3K14*. The sensor constructs were co-transfected either with miR-155 or backbone vectors. The obtained results revealed a significant reduction of the luciferase signals upon miR-155 co-transfection for *CEBBP*, *PHC2* and *MAP3K14* (**Fig. 3B**), which suggests that these genes are direct targets of miR-155, and a non-significant trend of reduction for *DUSP14*. We further quantified ZFP36 and DUSP14 protein levels upon transient miR-155 expression in HEK293T cells by western blot analyses. Thereby, we observed a significant reduction of ZFP36 protein by miR-155 of 0.3-fold and a less distinct effect of 0.5-fold and 0.8-fold for DUSP14 (**Fig. 3C**; **Fig. S7**), which confirms the results of the luciferase assays. Taken together, these data suggest that despite several putative miR-155 target transcripts were barely degraded, their protein levels were reduced, indicating translational repression as an important mode of miRNA-mediated regulation for a subset of targets.

We further analyzed whether the mode of miRNA activity correlates with seed sequence length or the amount of miR-155 binding sites by using the PITA prediction algorithm. For seed length determination we counted the longest seed interaction site, in case there were more than one predicted binding sites per transcript. Interestingly, we observed that the group of degraded miR-155 targets showed an enrichment for a seed length of 8 nucleotides (50% of targets) compared with the group of translationally inhibited targets (21%; **Fig. 3D**). Furthermore, the group of translationally repressed transcripts showed an enrichment for targets with just one putative miR-155 binding site (74% compared with 30% in the group of degraded targets). Whereas degraded transcripts contained more transcripts with four putative miR-155 binding sites (30% compared with 5% in the other group; **Fig. 3D**). Whether these observations can be explained by a dependency of the mode of miRNA activity on seed length and number of binding sites has to be clarified by more detailed analyses.

MicroRNA expression changes upon ectopic miR-155 expression. In order to delineate changes in the miRNA profile caused by ectopic expression of miR-155, TL and IP fractions of HEK-miR-155 and HEK-vector cells were analyzed by TaqMan arrays covering the 377 most frequently expressed miRNAs. In total, 248 and 193 miRNAs were detected in HEK-miR-155 IP and TL fractions, respectively. In HEK-vector cells, 249 miRNAs were detected in the IP fraction and 197 in the TL indicating an enrichment of miRNAs in AGO2 precipitates with an average difference of more than 3.5 Ct-values between IP and respective TL fraction. Comparison of the miRNA profiles of the TLs of the isogenic cell lines uncovered a differential expression of several miRNAs. For instance, miR-150 and miR-34a were expressed at higher levels in HEK-miR-155 cells with a ΔCt > 3. As expected, miR-155 was detected with a difference of more than six Ct-values, which confirmed our initial analysis using single plex miRNA assays (**Fig. 1A**). Furthermore, several miRNAs showed lower levels in HEK-miR-155 compared with HEK-vector cells. For instance miR-224, miR-135b and miR-98 levels were decreased with a difference of at least 2.5 Ct-values. Notably, no changes were observed for U6 snRNA controls measured as quadruplicates on the plates, indicating a robust detection with the TaqMan arrays. Furthermore, there were only minor variations in the levels of the housekeeping RNAs RNU44 (ΔCt < 0.15) and RNU48 (ΔCt < 0.08) between HEK-vector and HEK-miR-155 cells indicating equal amounts of starting material.

Table 1. Comparison of mRNAs and miRNAs in HEK-vector and HEK-miR-155 cells

	HEK-vector	HEK-miR-155
mRNAs with lower abundance in TL fraction	121	339
mRNAs with higher abundance in IP fraction	409	213
mRNAs with higher abundance in IP fraction after IP/TL normalization (predicted miR-155 targets)	0	100 (67)

The comparison of miRNAs with the highest abundance in the IP fractions of both isogenic cell lines revealed a large overlap, with 28 of the top 30 miRNAs in HEK-miR-155 IPs shared with HEK-vector IPs (**Fig. 4**). We further detected four miRNAs (miR-17, -222, -106a and -20a) with apparently higher abundance in the IP fractions compared with the ectopically expressed miR-155. Thus, we assume that the transgenic expression of miR-155 was near a physiologically relevant level. Furthermore, the relative abundance of the top 30 miRNAs, except for miR-155, was similar in both IP fractions, indicating that the miRNA machinery, including AGO2, was not affected or saturated and the activity of the most highly expressed miRNAs was not disturbed by the ectopic miR-155 expression (**Fig. 4**).

Disproportional loading of microRNAs into AGO2. MicroRNAs guide associated RISC complexes to their target mRNAs. Thus, in order to be functionally active, miRNAs have to be incorporated in an AGO protein. To investigate miRNA activity and to correlate it with its expression, we performed an integrated analysis of miRNA expression and corresponding enrichment profiles. As expected, we detected higher levels of miRNAs in the IP compared with the TL fractions. For the majority of miRNAs, levels were proportional in both fractions with constant IP to TL ratios. Interestingly, 20 and 18 miRNAs appeared to be over-proportionally enriched in the IP fractions of HEK-vector and HEK-miR-155 cells, respectively, with IP/TL ratios that were higher than the single standard deviation from the median values (HEK-vector: median-ratio 0.921, STDEV 0.09; HEK-miR-155: median-ratio 0.927, STDEV 0.084) (**Table 3**). In addition, 36 and 39 miRNAs were under-represented in the IP fractions, respectively. Furthermore, 35 of these miRNAs were commonly either over- or under-represented in the IP fractions of both isogenic cell lines.

To elucidate whether disproportional loading of miRNAs into RISC is a general phenomenon, we performed additional AGO2 IP experiments with two B-cell lines JEKO-1 and MEC-1 and again detected a disproportional abundance of miRNAs in the IP fractions, with 28 miRNAs showing disproportional IP/TL

Table 2. Predicted miR-155 target genes enriched in HEK-miR-155 IPs [log2 fold changes (FC) compared with HEK-vector IPs and p values are depicted]

Gene ID	Difference in log2 FC	*P* value
CEBPB*[18,27]	1.911	4.98E-05
DET1*[27]	1.734	2.99E-05
PHC2*[18]	1.581	9.97E-06
TCF4*[26]	1.570	8.97E-05
ZFP[36]	1.415	1.50E-04
AGTRAP*[46]	1.414	3.99E-05
MAP3K10	1.195	1.59E-04
CSNK1G2	1.112	3.19E-04
JARID2*[18]	1.025	2.59E-04
RAPGEF2	1.007	1.69E-04
TRIM32*[18]	1.007	1.30E-04
DHX40*[18]	0.932	1.20E-04
ZNF320	0.929	2.39E-04
VAMP3*[18]	0.893	2.49E-04
PSKH1	0.889	6.98E-05
ATP6V1G1	0.885	2.09E-04
IER5	0.873	4.49E-04
CNNM1	0.840	1.89E-04
TSHZ3*[47]	0.834	4.78E-04
C3orf18	0.817	7.48E-04
EN2	0.811	2.19E-04
DCK	0.792	1.79E-04
ARRDC2	0.770	5.28E-04
ZNF652*[27]	0.735	3.09E-04
BBS7	0.719	5.98E-04
EYA2	0.711	5.18E-04
ZNF468	0.699	9.77E-04
CTNND1	0.680	5.38E-04
ARVCF	0.679	1.13E-03
ATP6V1C1*[18]	0.673	3.49E-04
GALT	0.670	1.19E-03
TBC1D14	0.670	1.09E-03
DPY19L1	0.646	5.78E-04
MAP3K14	0.632	9.67E-04
NFIB	0.621	6.18E-04
RGL1	0.621	1.26E-03
PAK2	0.620	3.89E-04
BACH1*[27]	0.618	1.44E-03
DUSP14	0.617	6.88E-04
CARD10	0.613	4.09E-04
EID2	0.611	9.17E-04
RNF166	0.593	1.38E-03
FBXO9	0.582	3.59E-04

***,** experimentally verified miR-155 targets; **bold**, proliferation-related targets.

ratios, in each cell line (JEKO-1: median-ratio 0.892, STEDV 0.09; MEC-1: median-ratio 0.907, STDEV 0.088). Of these, 18 miRNAs, including several members of the miR-17-92 cluster, showed also disproportional values in HEK293T cells (**Fig. 5**). MiR-155, which was disproportionally enriched in the IP fraction of HEK-miR-155 cells, was also over-represented in JEKO-1 and MEC-1 IP fractions. Notably, the majority of over-proportionally enriched miRNAs were among the 50 most highly expressed miRNAs.

Taken together, our data underline the potential of RIP-Seq to identify the targetome of a specific miRNA or miRNomes. As part of the targetome of miR-155, we observed targets, which were regulated by translational repression as well as targets that underwent mRNA decay. We further provide evidence that the ectopic expression of miR-155 in HEK293T cells caused changes in the mRNA and miRNA expression profiles resulting in increased cell proliferation. In addition, we detected a recurrent, disproportional enrichment of miRNAs, including miR-155 and three members of the miR-17-92 cluster, by AGO2 IP.

Discussion

MicroRNA expression profiling and overexpression of selected miRNAs are tools, which are frequently used to investigate functionally relevant miRNA-mRNA interactions. In many studies, these techniques have been used with subsequent high-throughput profiling of mRNA decay to identify relevant miRNA targets. However, the mechanisms by which miRNAs regulate their targets are still a matter of debate, suggesting that translationally inhibited miRNA targets might be missed by these approaches. However, the enforced expression of miRNAs, a frequently used tool to characterize the function of miRNAs, induces also indirect changes within the mRNA and miRNA expression profile, which might contribute to the observed phenotypes. Furthermore, the dependency of miRNA expression and miRNA activity has been marginally addressed in the past. Recent studies suggest that a complex miRNA and target mRNA regulatory network is involved in the control of cellular phenotypes. Therefore, data providing insights into the global "miRNome" and "targetome" of cells are important for a better understanding of the functional role of miRNAs.

In the present study, we aimed at testing the accuracy of the RIP-Seq method under strictly defined conditions. We also used the obtained data to identify miR-155 target genes in a genome-wide approach and to investigate their functional relation. We therefore generated isogenic HEK293T cells with stable, ectopic expression of miR-155 that resulted in a significant increase in cell proliferation in comparison to the control cell line. These experiments allowed us to identify 67 known and novel, putative miR-155 targets in HEK-miR-155 cells. Of these, 17 were functionally related to proliferation. Enhancing effects of miR-155 on cell proliferation were also described in other cell types, e.g., B-cell lymphomas or breast cancer cells.[30,31]

Our data suggest that a combination of target genes, rather than a single miRNA-mRNA interaction, might be responsible for the observed enhanced cell proliferation, as e.g., knockdown

of the miR-155 target gene *CEBPB* resulted only in a minor increase of *CCND1*. A recently established computer model analyzing the global miRNome-targetome interaction network demonstrated the interdependent effects of mRNA expression and the cooperative fashion of miRNA-mediated gene regulation.[32] Moreover, findings about mRNAs, ncRNAs and pseudogenes[33-35] acting as endogenous modulators of miRNA activity by competing for miRNA binding underline the necessity to study miRNA activities in a global context.

The ectopic expression of miR-155 induced changes within the transcriptome, with more than 450 significantly altered mRNAs including 339 downregulated and 121 upregulated genes. Of these, merely 21.5% and 11.6% were predicted as direct miR-155 targets, respectively. Furthermore, 622 transcripts were differentially enriched in the IPs with 409 and 213 mRNAs showing significantly different co-precipitation in HEK-vector and HEK-miR-155 cells, respectively. Of these, 18.3% and 13.7% were predicted as miR-155 targets, respectively. In our previous study using the SILAC approach, we identified 46 proteins which were downregulated upon transient miR-155 expression in HEK293T cells. Thirteen of these showed a tendency for transcript degradation in the TL or an enrichment in the IP fraction of HEK-miR-155 cells.[36] However, these studies were performed using transiently transfected cells and the experimental design was not restricted to de novo synthesized proteins, which might limit the number of commonly identified targets. Taken together, these data indicate that the overexpression of a single miRNA causes, besides regulation of its direct targets, a secondary modulation of a broad spectrum of genes and miRNAs, which might be involved in the observed phenotypic changes and which should be considered for experimental set-ups with enforced miRNA overexpression. Of note, by performing TaqMan arrays, we could show that the stable ectopic expression of miR-155 in our experiments was within a physiologic range, as several endogenous miRNAs were expressed at higher levels and the AGO2-miRNA interaction profile for the most highly expressed miRNAs was similar to the control.

In order to account for secondary gene alterations caused by enforced miR-155 expression, we normalized the mRNA profiles of the IP fractions with the corresponding TLs, which revealed 100 potential miR-155 target genes in HEK-miR-155 cells and not a single altered mRNA in HEK-vector cells. Sixty-seven of these 100 transcripts were in silico predicted miR-155 targets. However, miRNA target prediction algorithms harbor the uncertainties of false-negative and false-positive results. We therefore followed a conservative strategy by solely counting putative targets, which were identified by at least three out of five commonly used algorithms. Notably, using TargetScan for single target prediction revealed exactly the same 67 miR-155 targets, which were identified by the combined approach. As recent publications suggested additional miRNA interactions with the 5'UTR, coding sequence of the target as well as non-canonical interaction of miRNAs and their target sequences,[37,38] we screened the remaining 33 transcripts with the RNA22 prediction algorithm, which is capable of detecting targets in the 5'UTR as well as coding sequences. Accordingly, we identified unique miR-155 interaction sites for seven of these genes.

Table 2. Predicted miR-155 target genes enriched in HEK-miR-155 IPs [log2 fold changes (FC) compared with HEK-vector IPs and p values are depicted]

LDLRAP1	0.579	7.58E-04
TRIP13*[18]	0.578	9.07E-04
MASTL	0.560	5.68E-04
CDC42EP4	0.557	8.27E-04
TMTC2	0.551	1.63E-03
FOS*[46]	0.550	1.27E-03
BRWD1	0.540	8.47E-04
ARFIP1*[18]	0.535	9.27E-04
TAPT1	0.533	1.72E-03
TUSC1	0.512	6.38E-04
RCN2*[18]	0.505	1.96E-03
RAB34*[18]	0.504	9.37E-04
TSPAN14	0.469	1.18E-03
C2orf18	0.447	1.70E-03
CHAF1A*[18]	0.436	1.28E-03
EIF5A2	0.425	1.81E-03
ANKFY1*[18]	0.422	1.52E-03
MPP5	0.421	1.83E-03
SMAD5*[27]	0.417	1.53E-03
STK38	0.417	1.50E-03
LRP12	0.410	1.60E-03
GNE	0.390	1.97E-03
AHRR	0.390	1.10E-03
PDK1	0.365	1.54E-03

***,** experimentally verified miR-155 targets; **bold**, proliferation-related targets.

Of the 67 potential miR-155 targets identified by RIP-Seq, 20 showed a significant enrichment in the IP and no significant ($p < 0.05$) change in the TL fraction (e.g., *PHC2* and *DUSP14*), suggesting that these transcripts were primarily regulated by translational repression and would not have been identified by expression profiling, as indicated by the subsequent qRT-PCR analyses. However, luciferase sensor assays and western blot analyses confirmed two of these genes, *DUSP14* and *PHC2,* as direct miR-155 targets on protein level. Strikingly, according to the pSILAC database (psilac.mdc-berlin.de), PHC2 was identified as a miR-155 target on protein level, however the changes on mRNA levels in that study were very weak with a fold change of 0.97.[18] The reduction of DUSP14 protein levels were moderate as seen by western blot and luciferase assays, reflecting the relatively mild but significant enrichment in the AGO2 IPs, which indicates that RIP-Seq is a more sensitive method for the identification of miRNA targts. Only nine identified miR-155 targets (e.g., *BACH1* and *JARID2*) showed a significant ($p < 0.05$) decay of mRNA in the TL fraction as confirmed by qRT-PCR. The majority of putative miR-155 targets showed, however, a modest

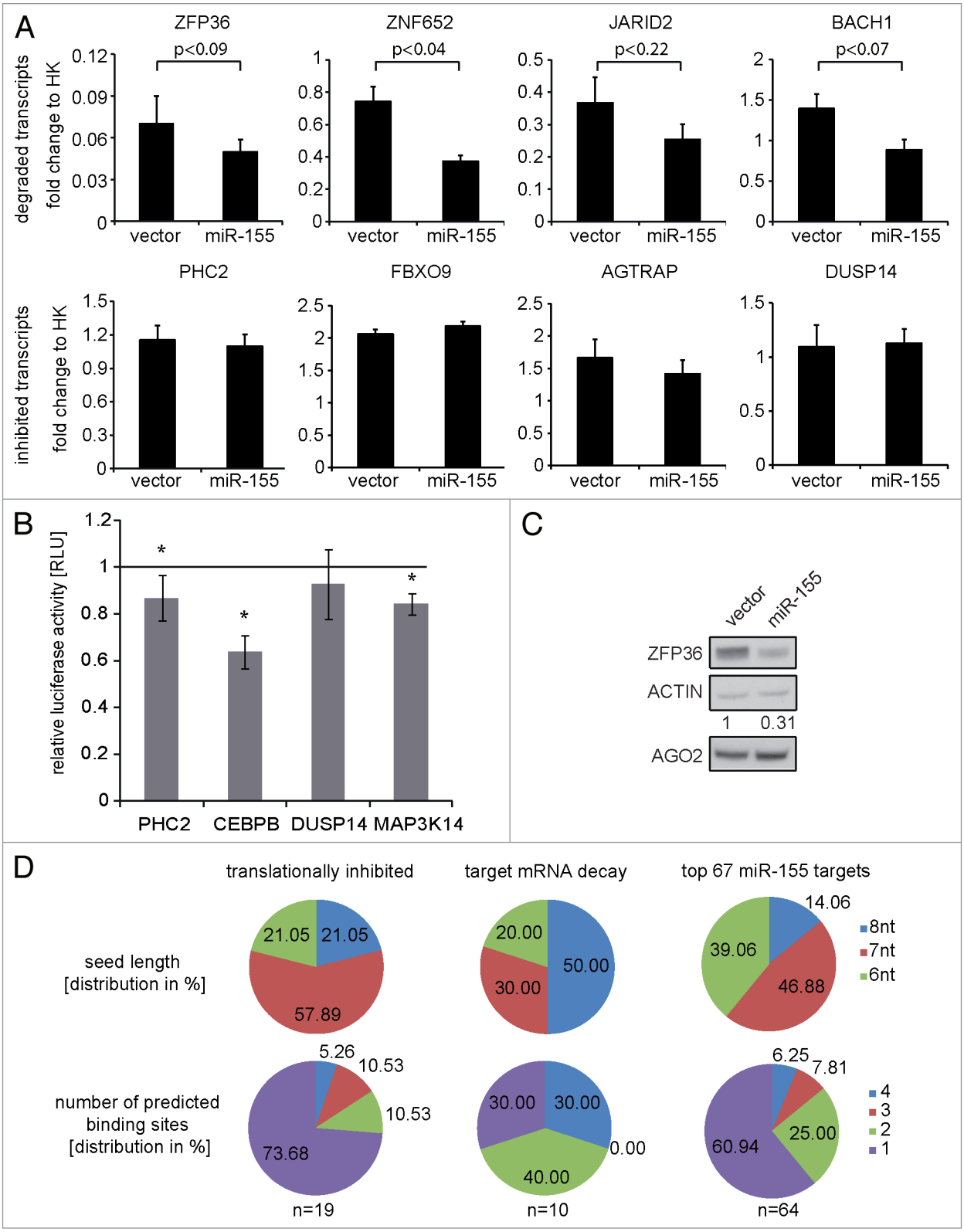

Figure 3. Validation of miR-155 targets on transcript and protein level. (**A**) Quantification of transcripts from 4 transcriptionally degraded and four translationally repressed miR-155 targets by qRT-PCR in HEK-vector and HEK-mir-155 cells. Ct-values were normalized to the mean of two housekeeping genes *GAPDH* and *DCTN2* (HK). Relative transcript levels of HEK-vector and HEK-miR-155 cells are depicted. (**B**) Luciferase sensor assays of miR-155 targets identified by RIP-Seq. The control experiments without miR-155 expression were set to 1 (black line). Statistical significance was calculated by student's t-test (* = $p < 0.05$). (**C**) Western blot analysis of ZFP36 and AGO2 protein expression in HEK cells with and without enforced miR-155 expression. Equal loading of protein lysates was confirmed by β-Actin detection. (**D**) Correlation of seed length and number of putative miR-155 binding sites per transcript to the mode of miRNA-mediated target regulation as predicted by the PITA algorithm.

enrichment in the IP fraction and a weak, non-significant degradation in the corresponding TL. The correlation of seed length and the amount of predicted miRNA-binding sites per transcript indicated a trend for longer seed sequences and more binding sites within the group of degraded miR-155 targets.

Even though we investigated changes of the transcriptome and targetome at a steady-state level and enzymatic activities should be inhibited during cell lysis and IP, we might have missed targets, which are extremely fast and completely degraded upon RISC binding. Such transcripts might not be detected in the IP fractions and will therefore be missed by this technique.

We observed a strong increase of *CCND1* mRNA in the TL of HEK-miR-155 cells partly caused by the miR-155-mediated reduction of the transcription factor CEBPB. In addition, we found *CCND1* mRNA enriched in the IPs of HEK-miR-155 cells. We assume that *CCND1* was enriched in the IP fraction because it was bound by endogenously expressed miRNAs, like miR-17 and miR-106a,[16,17] indicating the importance to adjust the IP profiles for secondary gene expression changes in this experimental setting.

Taken together, these observations support the general idea of a combined mode of miRNA activity to regulate gene expression, including miRNA-mediated target decay and translational inhibition, as described by others.[39] The usage of techniques like RIP-Seq increases the dynamic range and accuracy of target identification, allowing the determination of targets by screening for transcript degradation in the TL and relative enrichment in the IP, which identifies degraded and translationally inhibited miRNA targets. Furthermore, combining the effects on the TL and IP level provides the ability to distinguish primary targets from secondary changes in the cellular transcriptome and targetome as an indirect consequence of ectopic miRNA expression.

MicroRNA expression profiling is a commonly used tool to characterize their role in diseases like cancer. However, miRNAs are only active when incorporated into RISC complexes. In this work we therefore addressed, whether miRNA expression profiles reflect the actual activity of miRNAs by comparing miRNA profiles of TL and IP fractions. We observed a disproportional association of several miRNAs with AGO2 including miR-155, miR-17, miR-20a, miR-92a and miR-106a. This is in accordance with data recently published by Goff et al.,[12] who reported over-proportional abundance of several miRNAs in AGO2 IPs of neuronal stem cells, including miR-320, which was also over-represented in all cell lines tested in our study.[12] Interestingly, Burroughs et al. reported that snRNAs U1 and U2 were associated with AGO proteins.[40] We detected an AGO2 association of snRNA U6, which was, similar as for several miRNAs, under-represented in relation to the TL levels in cell lines tested (not shown). Whether these observations have an impact on target gene regulation has to be addressed in future studies. Furthermore, the mechanisms, which are responsible for this effect, remain elusive. Feasible explanations are variations in AGO2-miRNA stabilities, different miRNA accessibilities due to sub-cellular distribution, miRNA-specific AGO2 loading efficiencies or a differential expression of co-factors involved in miRNA loading processes. Whether this observation is restricted to AGO2 or resembles a general feature of all AGO proteins needs to be further investigated. Two studies, in which miRNA profiles of AGO1-3 IPs were compared, indicate mild loading biases for a limited number of miRNAs. The results of these studies suggest an involvement of miRNA length in AGO protein specificity.[40,41]

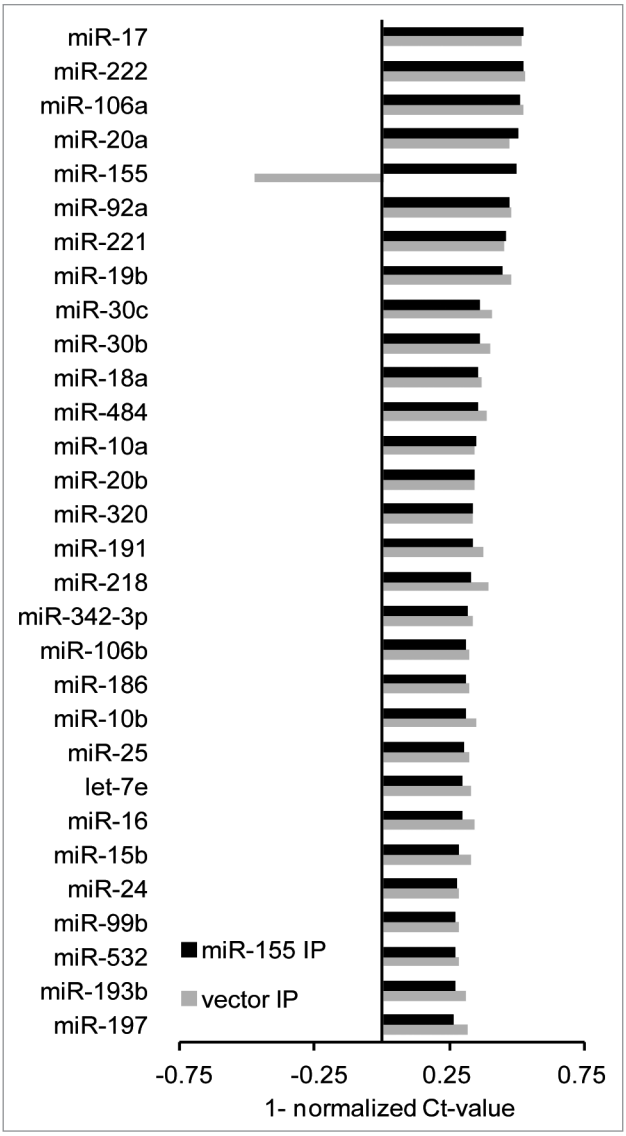

Figure 4. Top 30 miRNAs detected in AGO2 IPs of HEK-miR-155 cells. Normalized Ct-values (ΔΔCt) obtained by TaqMan arrays of the 30 most abundant miRNAs in the IP fraction of HEK-miR-155 cells were compared in HEK-miR-155 (black) and HEK-vector (gray) IP fractions.

Considering the findings of our study and data presented by other groups, we suggest that classical miRNA expression profiling might not necessarily reflect the de facto activity of miRNAs as recently proposed also by Mullokandov and colleagues.[42]

Materials and Methods

Cell culture and generation of stable cell lines. The cell line HEK293T (CRL-1573) was received from the American Type

Table 3. MicroRNAs with overproportional IP to TL ratios (ΔΔCt-values relative to the median are depicted, smaller numbers indicate a relatively higher abundance of the respective miRNA)

HEK-vector	Relative Ct-values	HEK-miR-155	Relative Ct-values
hsa-miR-222	0.728	hsa-miR-155	0.739
hsa-miR-92a	0.733	hsa-miR-222	0.746
hsa-miR-221	0.762	hsa-miR-92a	0.753
hsa-miR-106a	0.777	hsa-miR-501–3p	0.755
hsa-miR-17	0.784	hsa-miR-221	0.774
hsa-miR-320	0.790	hsa-miR-320	0.775
hsa-miR-342–3p	0.792	hsa-miR-17	0.787
hsa-miR-197	0.799	hsa-miR-342–3p	0.797
hsa-miR-615–5p	0.804	hsa-miR-20a	0.807
hsa-miR-191	0.809	hsa-miR-10a	0.809
hsa-miR-20a	0.815	hsa-miR-615–5p	0.815
hsa-let-7e	0.818	hsa-miR-106a	0.828
hsa-miR-10b	0.818	hsa-miR-191	0.829
hsa-miR-30b	0.818	hsa-miR-125a-3p	0.832
hsa-miR-501	0.821	hsa-miR-125a-5p	0.835
hsa-miR-30c	0.826	hsa-miR-197	0.838
hsa-miR-99b	0.828	hsa-miR-425–5p	0.841
hsa-miR-346	0.830	hsa-miR-99b	0.841
hsa-miR-10a	0.830		
hsa-miR-125a-5p	0.830		

Culture Collection (ATCC), MEC-1 (ACC 497) and JEKO-1 (ACC 553) from the German Resource Centre for Biological Material (DSMZ). HEK293T and MEC-1 were cultured in Dulbecco's modified Eagle medium (DMEM) containing 10% fetal bovine serum (FBS), and 1% penicillin/streptomycin. JEKO-1 was cultured in RPMI-1640 containing 20% FBS and 1% penicillin/streptomycin. The cells were incubated at 37°C, 95% humidity and 5% (for RPMI) or 10% (for DMEM) CO_2.

For transgenic miR-155 expression, the pre-miR-155 sequence was amplified using genomic DNA of MEC-1 cells and the primers listed in **Table S5**. The amplified fragment was ligated into the episomal. Vector pREP4 (Invitrogen) using Hind III and Xho I restriction sites. The resulting pREP4miR-155 vector was Sanger sequenced to test for mutations and proper integration of the pre-miR-155 sequence. To generate HEK293T cells with ectopic, stable expression of miR-155, 5×10^6 cells were transfected with 2 μg of pREP4-miR-155 using TransIT-LT1 transfection reagent (Mirus bio LLC). Cells transfected with the pREP4 vector backbone were generated accordingly. Transfected cells were selected with 250 μg/ml hygromycin B (Invitrogen) for 4 wk while passaged every second day. To monitor transgenic expression of miR-155, quantitative reverse transcription-PCR was performed at several time points.

Transfection of siRNAs in HEK293T cells was performed using HiPerfect transfection reagent (Qiagen) according to the manufacturer's instructions.

Quantification of mRNA and miRNA. For mRNA quantification, total RNA was isolated using the miRNeasy kit (Qiagen) and reverse transcribed using Superscript II and random primer (Invitrogen) according to the manufacturer's instructions. Amplification and quantification of cDNA was performed in 7900 HT Fast Real-Time PCR System (Applied Biosystems) in triplicates using SYBR Green (Thermo Scientific) according to the manufacturer's protocol and as described before.[43] Relative quantities were calculated in relation to the housekeeping genes (*GAPDH, DCTN2*). The qPCR primer sequences are listed in **Table S5**.

Quantitative RT-PCR analysis of miRNAs was performed using RNA isolated by miRNeasy kit (Qiagen) and TaqMan MicroRNA Assays (Applied Biosystems). Relative amounts of miRNAs were calculated in relation to the house keeping small RNA RNU-6B.

MicroRNA expression profiles were generated using TaqMan Array System version 3 (Applied Biosystems) according to the manufacturer's protocol. After reverse transcription of 20 ng RNA isolated by the RIP protocol, cDNA was pre-amplified, detected and quantified using TaqMan Array "A" cards. Ct-values higher than 35 were considered as not expressed. Ct-values were normalized to the median value of all expressed miRNAs in the respective sample (ΔCt).

RNA-interacting protein IP (RIP)-Seq. Cells (2×10^8 – 4×10^8 per IP) were washed with ice-cold PBS and lysed in 400 μl polysome lysis buffer (PLB)[13] for 5 min on ice and freezing at –80°C. Protein G sepharose (GE Healthcare Europe GmbH; 50 μl per tube) was coupled to a mixture of 5 μg each of two AGO2-specific antibodies (Abnova, clone 2E12-1C9; Sigma Aldrich, clone 11A9) or 10 μg IgG1 isotype control antibody (Jackson Immunoresearch laboratories) in 500 μl NT2 buffer[13] in low binding tubes for 1 h at 4°C, followed by three washing steps with NT2 buffer. Thawed lysates were centrifuged at 13,000 rpm and 4°C for 10 min, added 1:10 to NT2-buffer containing 5 μl RNaseOUT (Invitrogen), 2 μl vanadyl ribonucleoside complex (New England Biolabs), 10 μl of 100 mM DTT (Invitrogen), 10 μl of 25 mM EDTA (Invitrogen) and 10 μl protease inhibitor cocktail (Roche) per 1 ml buffer. Of this mixture 100 μl were recovered as total lysate fraction (TL). The remaining lysate was portioned equally to four tubes containing AGO2-antibody coated beads and incubated for one hour at 4°C. Thereafter, the beads were collected by centrifugation, the supernatant (SN) was stored at –80°C for later use, and the sepharose beads were washed five times in 1 ml of NT2-buffer, prior to elution of bound protein by incubation in 50 μl of 1 M glycine (pH 2.3) at room temperature for 10 min, followed by neutralization using 5 μl of 1 M TRIS-HCl (pH 8). Proteins were then degraded by adding 3 μl of proteinase K (Qiagen), and RNA was isolated using 350 μl TRIZOL LS reagent (Invitrogen) followed by miRNeasy kit (Qiagen) purification.

Luciferase sensor assays. For luciferase sensor assays 3×10^4 HEK293T cells were co-transfected with pMiRReport vector containing the 3'UTR of the target gene of interest, a TK renilla vector and either the miR-155 overexpressing or the corresponding control vector using TransIT-LT1 transfection reagent

(Mirus Bio). The cells were lysed 24 h after transfection using 65 μl of passive lysis buffer (Promega). Luciferase signals were detected on a Mithras 96-well plate reader (Berthold technologies) using a custom made dual luciferase buffer system[44] and 20 μl of the protein lysate. All measurements were performed as triplactes. The firefly luciferase signals were normalized to the respective *renilla* signals. Control experiments without ectopic miR-155 expression were scaled to 1. All experiments were performed in three biological replicates.

Western blot analyses. HEK293T cells were lysed 48 h after transfection with miR-155 or control vector, using RIPA buffer, containing EDTA-free proteinase inhibitor complete mini (Roche) and Benzonase (Merck). Cellular debris was removed by spinning the lysates. Protein concentrations were tested by BCA assays (Pierce). Equal amounts of each lysate were loaded onto a denaturing poly-acrylamide gel. The proteins were size-separated and transferred to a PVDF-membrane (Merck). DUSP14 protein was detected using a monoclonal antibody (clone 4B5-E6, Abnova coporation). ZFP36 was detected using a polyclonal antibody (ABE285, Merck Millipore). The AGO2 protein was detected by mouse monoclonal antibody (clone 2E12-1C9). A polyclonal antibody against β-Actin (clone sc-1616, Santa Cruz) was used as loading control. Both antibodies were detected using HRP-linked secondary antibodies against mouse or rabbit, respectively (Cell signaling technology) and ECL plus detection chemistry (GE Healthcare). The DUSP14 signal was removed by incubating the membrane for 30 min with 0.1% sodium-azide in PBS prior to β-Actin detection.

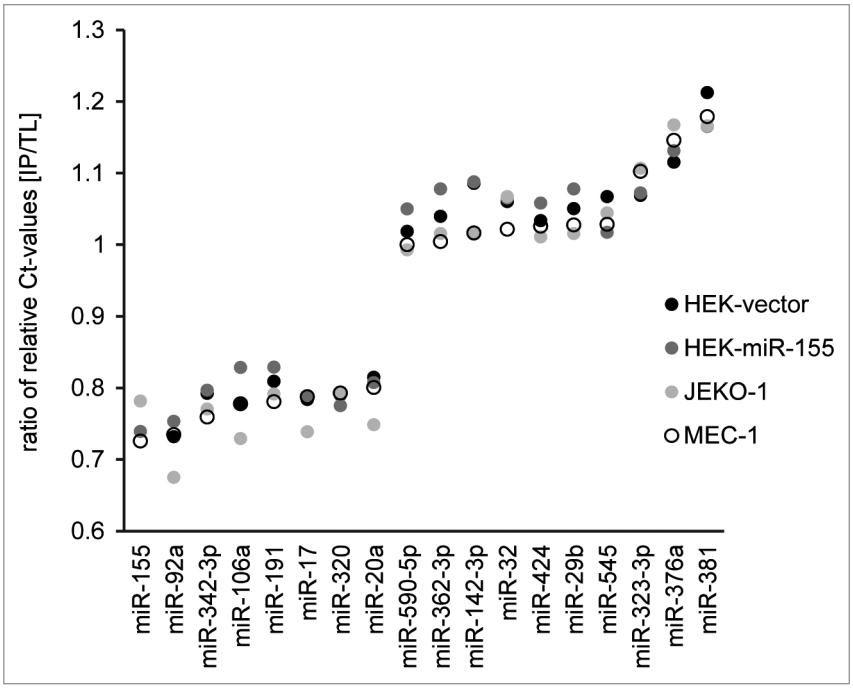

Figure 5. Comparison of miRNA levels in IP and respective TL fractions. RIP experiments followed by miRNA TaqMan arrays of IP and TL fractions of HEK-miR-155, HEK-vector, JEKO-1 and MEC-1 cells were performed and ratios of relative Ct-values (ΔΔCt) of IP vs. TL samples were calculated. All miRNAs displaying a recurrent, disproportional enrichment or depletion in the IP vs. TL fractions are depicted.

High-throughput sequencing. The RNA fraction isolated by RIP was quantified by NanoDrop analysis and its quality was assessed by Agilent capillary electrophoresis using the RNA picoChips and the setting for total RNA analysis. The sequencing libraries were generated using 300–600 ng of RNA and the TruSeq mRNA sequencing Kit from Illumina according to the manufacturer's instructions. Briefly, the RNA samples were poly-A purified using oligo-dT beads. The RNA was enzymatically degraded using endoribonucleases generating small fragments of approximately 200 bp in length. The cDNA synthesis was performed by first strand synthesis followed by second strand synthesis. After end repair and 3' end adenylation, the sequencing adaptor oligo mix was ligated to the unstranded cDNA library. In order to perform a multiplexed sequencing run, six different barcoded sequencing adaptors were used. The cDNA library was amplified using 15 cycles of PCR according to the manufacturer's manual (Illumina). The enrichment and size distribution of the libraries were tested by Agilent capillary gel electrophoresis on a DNA1000 chip. For sequencing, six samples were pooled at equal molarities per lane. Nine pmol of each sample library pool were loaded per lane of an Illumina version 3 single read flow cell. The hybridization and cluster generation was performed on a cBot unit. The samples were single-end sequenced with a read length of 51 bp on an Illumina HiSeq 2000 sequencer. Raw data were sorted and analyzed according to barcoded library adaptors allowing one basepair mismatch within the barcode sequence. Absolute read counts are depicted in **Table S6**.

Sequencing reads were mapped against the human reference genome version 19 using the TopHat algorithm version 1.4.0[15] supplying Ensembl gene annotations version GRCh37.65 and default settings. RNA levels of 20,318 protein-coding genes were calculated using the HTSeq-Count algorithm version 0.5.3p3 and default settings except defining unstranded sequencing libraries.[45]

Further analysis was performed using the R statistical programming language version 2.15.0. Default settings were used unless otherwise noted. Testing for genes differentially enriched between the IP and total lysate fractions of both cell lines was performed using the functions "estimateSizeFactors" and "nbinomTest" from the DESeq package version 1.8.2. Log2-ratios of IP and total lysate fractions from the same biological sample were calculated for genes with an average normalized read count of at least 250 (10,036 genes). The resulting ratios were normalized using the function "normalizeQuantiles" from the limma package version 1.32.0 and tested for differential enrichment between HEK-miR-155 and HEK-vector cells using the Significance Analysis of Microarrays (SAM) method from the siggenes package version 1.30.0.

Disclosure of Potential Conflicts of Interest

No potential conflicts of interest were disclosed.

Acknowledgments

The authors thank Angela Schulz, Sibylle Ohl and Verena Kalter for experimental support. We thank Thorsten Kolb, Angela Schulz, Daniel Haag and Verena Thewes for helpful discussions and André Leischwitz, Berit Haldemann and Stephan Wolf for next-generation sequencing support. Furthermore, we thank Thore Kempf and Martina Schnölzer for the mass spec analyses. We thank Sven Diederichs for critically reading and discussing the manuscript.

Research Support

This study was supported by a grant from the Deutsche José Carreras Leukämie-Stiftung (DJCLS R 10/04), by the research project of the German Federal Ministry of Education and Research "CancerEpiSys" and by the Helmholtz Virtual Institute "Understanding and overcoming resistance to apoptosis and therapy in leukemia."

Supplemental Material

Supplemental material may be found here:
http://www.landesbioscience.com/journals/rnabiology/article/24553/

References

1. Bartel DP. MicroRNAs: genomics, biogenesis, mechanism, and function. Cell 2004; 116:281-97; PMID:14744438; http://dx.doi.org/10.1016/S0092-8674(04)00045-5.
2. Izaurralde E. Elucidating the temporal order of silencing. EMBO Rep 2012; 13:662-3; PMID:22722480; http://dx.doi.org/10.1038/embor.2012.91.
3. Béthune J, Artus-Revel CG, Filipowicz W. Kinetic analysis reveals successive steps leading to miRNA-mediated silencing in mammalian cells. EMBO Rep 2012; 13:716-23; PMID:22677978; http://dx.doi.org/10.1038/embor.2012.82.
4. Braun JE, Huntzinger E, Fauser M, Izaurralde E. GW182 proteins directly recruit cytoplasmic deadenylase complexes to miRNA targets. Mol Cell 2011; 44:120-33; PMID:21981923; http://dx.doi.org/10.1016/j.molcel.2011.09.007.
5. Chekulaeva M, Mathys H, Zipprich JT, Attig J, Colic M, Parker R, et al. miRNA repression involves GW182-mediated recruitment of CCR4-NOT through conserved W-containing motifs. Nat Struct Mol Biol 2011; 18:1218-26; PMID:21984184; http://dx.doi.org/10.1038/nsmb.2166.
6. Filipowicz W, Bhattacharyya SN, Sonenberg N. Mechanisms of post-transcriptional regulation by microRNAs: are the answers in sight? Nat Rev Genet 2008; 9:102-14; PMID:18197166; http://dx.doi.org/10.1038/nrg2290.
7. Fabian MR, Cieplak MK, Frank F, Morita M, Green J, Srikumar T, et al. miRNA-mediated deadenylation is orchestrated by GW182 through two conserved motifs that interact with CCR4-NOT. Nat Struct Mol Biol 2012; 19:364; PMID:21984185; http://dx.doi.org/10.1038/nsmb0312-364c.
8. Costinean S, Sandhu SK, Pedersen IM, Tili E, Trotta R, Perrotti D, et al. Src homology 2 domain-containing inositol-5-phosphatase and CCAAT enhancer-binding protein beta are targeted by miR-155 in B cells of Emicro-MiR-155 transgenic mice. Blood 2009; 114:1374-82; PMID:19520806; http://dx.doi.org/10.1182/blood-2009-05-220814.
9. Vigorito E, Perks KL, Abreu-Goodger C, Bunting S, Xiang Z, Kohlhaas S, et al. microRNA-155 regulates the generation of immunoglobulin class-switched plasma cells. Immunity 2007; 27:847-59; PMID:18055230; http://dx.doi.org/10.1016/j.immuni.2007.10.009.
10. Wang WX, Wilfred BR, Hu Y, Stromberg AJ, Nelson PT. Anti-Argonaute RIP-Chip shows that miRNA transfections alter global patterns of mRNA recruitment to microribonucleoprotein complexes. RNA 2010; 16:394-404; PMID:20042474; http://dx.doi.org/10.1261/rna.1905910.
11. Easow G, Teleman AA, Cohen SM. Isolation of microRNA targets by miRNP immunopurification. RNA 2007; 13:1198-204; PMID:17592038; http://dx.doi.org/10.1261/rna.563707.
12. Goff LA, Davila J, Swerdel MR, Moore JC, Cohen RI, Wu H, et al. Ago2 immunoprecipitation identifies predicted microRNAs in human embryonic stem cells and neural precursors. PLoS One 2009; 4:e7192; PMID:19784364; http://dx.doi.org/10.1371/journal.pone.0007192.
13. Tan LP, Seinen E, Duns G, de Jong D, Sibon OC, Poppema S, et al. A high throughput experimental approach to identify miRNA targets in human cells. Nucleic Acids Res 2009; 37:e137; PMID:19734348; http://dx.doi.org/10.1093/nar/gkp715.
14. Hoffman AE, Liu R, Fu A, Zheng T, Slack FJ, Zhu Y. Targetome profiling, pathway analysis and genetic association study implicate miR-202 in lymphomagenesis. Cancer Epidemiol Biomarkers Prev 2013; 22:327-36; PMID:23334589; http://dx.doi.org/10.1158/1055-9965.EPI-12-1131-T.
15. Trapnell C, Pachter L, Salzberg SL. TopHat: discovering splice junctions with RNA-Seq. Bioinformatics 2009; 25:1105-11; PMID:19289445; http://dx.doi.org/10.1093/bioinformatics/btp120.
16. Deshpande A, Pastore A, Deshpande AJ, Zimmermann Y, Hutter G, Weinkauf M, et al. 3'UTR mediated regulation of the cyclin D1 proto-oncogene. Cell Cycle 2009; 8:3584-92; PMID:19823025; http://dx.doi.org/10.4161/cc.8.21.9993.
17. Qin X, Wang X, Wang Y, Tang Z, Cui Q, Xi J, et al. MicroRNA-19a mediates the suppressive effect of laminar flow on cyclin D1 expression in human umbilical vein endothelial cells. Proc Natl Acad Sci USA 2010; 107:3240-4; PMID:20133739; http://dx.doi.org/10.1073/pnas.0914882107.
18. Selbach M, Schwanhäusser B, Thierfelder N, Fang Z, Khanin R, Rajewsky N. Widespread changes in protein synthesis induced by microRNAs. Nature 2008; 455:58-63; PMID:18668040; http://dx.doi.org/10.1038/nature07228.
19. Gutsch R, Kandemir JD, Pietsch D, Cappello C, Meyer J, Simanowski K, et al. CCAAT/enhancer-binding protein beta inhibits proliferation in monocytic cells by affecting the retinoblastoma protein/E2F/cyclin E pathway but is not directly required for macrophage morphology. J Biol Chem 2011; 286:22716-29; PMID:21558273; http://dx.doi.org/10.1074/jbc.M110.152538.
20. Kertesz M, Iovino N, Unnerstall U, Gaul U, Segal E. The role of site accessibility in microRNA target recognition. Nat Genet 2007; 39:1278-84; PMID:17893677; http://dx.doi.org/10.1038/ng2135.
21. Betel D, Koppal A, Agius P, Sander C, Leslie C. Comprehensive modeling of microRNA targets predicts functional non-conserved and non-canonical sites. Genome Biol 2010; 11:R90; PMID:20799968; http://dx.doi.org/10.1186/gb-2010-11-8-r90.
22. Grimson A, Farh KK, Johnston WK, Garrett-Engele P, Lim LP, Bartel DP. MicroRNA targeting specificity in mammals: determinants beyond seed pairing. Mol Cell 2007; 27:91-105; PMID:17612493; http://dx.doi.org/10.1016/j.molcel.2007.06.017.
23. Maragkakis M, Reczko M, Simossis VA, Alexiou P, Papadopoulos GL, Dalamagas T, et al. DIANA-microT web server: elucidating microRNA functions through target prediction. Nucleic Acids Res 2009; 37(Web Server issue):W273-6; PMID:19406924; http://dx.doi.org/10.1093/nar/gkp292.
24. Maragkakis M, Alexiou P, Papadopoulos GL, Reczko M, Dalamagas T, Giannopoulos G, et al. Accurate microRNA target prediction correlates with protein repression levels. BMC Bioinformatics 2009; 10:295; PMID:19765283; http://dx.doi.org/10.1186/1471-2105-10-295.
25. Lewis BP, Burge CB, Bartel DP. Conserved seed pairing, often flanked by adenosines, indicates that thousands of human genes are microRNA targets. Cell 2005; 120:15-20; PMID:15652477; http://dx.doi.org/10.1016/j.cell.2004.12.035.
26. Xiang X, Zhuang X, Ju S, Zhang S, Jiang H, Mu J, et al. miR-155 promotes macroscopic tumor formation yet inhibits tumor dissemination from mammary fat pads to the lung by preventing EMT. Oncogene 2011; 30:3440-53; PMID:21460854; http://dx.doi.org/10.1038/onc.2011.54.
27. Yin Q, McBride J, Fewell C, Lacey M, Wang X, Lin Z, et al. MicroRNA-155 is an Epstein-Barr virus-induced gene that modulates Epstein-Barr virus-regulated gene expression pathways. J Virol 2008; 82:5295-306; PMID:18367535; http://dx.doi.org/10.1128/JVI.02380-07.
28. Bazzini AA, Lee MT, Giraldez AJ. Ribosome profiling shows that miR-430 reduces translation before causing mRNA decay in zebrafish. Science 2012; 336:233-7; PMID:22422859; http://dx.doi.org/10.1126/science.1215704.
29. Djuranovic S, Nahvi A, Green R. miRNA-mediated gene silencing by translational repression followed by mRNA deadenylation and decay. Science 2012; 336:237-40; PMID:22499947; http://dx.doi.org/10.1126/science.1215691.
30. Willimott S, Wagner SD. miR-125b and miR-155 contribute to BCL2 repression and proliferation in response to CD40 ligand (CD154) in human leukemic B-cells. J Biol Chem 2012; 287:2608-17; PMID:22139839; http://dx.doi.org/10.1074/jbc.M111.285718.
31. Jiang S, Zhang HW, Lu MH, He XH, Li Y, Gu H, et al. MicroRNA-155 functions as an OncomiR in breast cancer by targeting the suppressor of cytokine signaling 1 gene. Cancer Res 2010; 70:3119-27; PMID:20354188; http://dx.doi.org/10.1158/0008-5472.CAN-09-4250.
32. Sumazin P, Yang X, Chiu HS, Chung WJ, Iyer A, Llobet-Navas D, et al. An extensive microRNA-mediated network of RNA-RNA interactions regulates established oncogenic pathways in glioblastoma. Cell 2011; 147:370-81; PMID:22000015; http://dx.doi.org/10.1016/j.cell.2011.09.041.

33. Poliseno L, Salmena L, Zhang JW, Carver B, Haveman WJ, Pandolfi PP. A coding-independent function of gene and pseudogene mRNAs regulates tumour biology. Nature 2010; 465:1033-8; PMID:20577206; http://dx.doi.org/10.1038/nature09144.
34. Ebert MS, Sharp PA. Emerging roles for natural microRNA sponges. Curr Biol 2010; 20:R858-61; PMID:20937476; http://dx.doi.org/10.1016/j.cub.2010.08.052.
35. Arvey A, Larsson E, Sander C, Leslie CS, Marks DS. Target mRNA abundance dilutes microRNA and siRNA activity. Mol Syst Biol 2010; 6:363; PMID:20404830; http://dx.doi.org/10.1038/msb.2010.24.
36. Lössner C, Meier J, Warnken U, Rogers MA, Lichter P, Pscherer A, et al. Quantitative proteomics identify novel miR-155 target proteins. PLoS One 2011; 6:e22146; PMID:21799781; http://dx.doi.org/10.1371/journal.pone.0022146.
37. Hafner M, Landthaler M, Burger L, Khorshid M, Hausser J, Berninger P, et al. Transcriptome-wide identification of RNA-binding protein and microRNA target sites by PAR-CLIP. Cell 2010; 141:129-41; PMID:20371350; http://dx.doi.org/10.1016/j.cell.2010.03.009.
38. Loeb GB, Khan AA, Canner D, Hiatt JB, Shendure J, Darnell RB, et al. Transcriptome-wide miR-155 binding map reveals widespread noncanonical microRNA targeting. Mol Cell 2012; 48:760-70; PMID:23142080; http://dx.doi.org/10.1016/j.molcel.2012.10.002.
39. Hendrickson DG, Hogan DJ, Herschlag D, Ferrell JE, Brown PO. Systematic identification of mRNAs recruited to argonaute 2 by specific microRNAs and corresponding changes in transcript abundance. PLoS One 2008; 3:e2126; PMID:18461144; http://dx.doi.org/10.1371/journal.pone.0002126.
40. Burroughs AM, Ando Y, de Hoon MJ, Tomaru Y, Suzuki H, Hayashizaki Y, et al. Deep-sequencing of human Argonaute-associated small RNAs provides insight into miRNA sorting and reveals Argonaute association with RNA fragments of diverse origin. RNA Biol 2011; 8:158-77; PMID:21282978; http://dx.doi.org/10.4161/rna.8.1.14300.
41. Dueck A, Ziegler C, Eichner A, Berezikov E, Meister G. microRNAs associated with the different human Argonaute proteins. Nucleic Acids Res 2012; 40:9850-62; PMID:22844086; http://dx.doi.org/10.1093/nar/gks705.
42. Mullokandov G, Baccarini A, Ruzo A, Jayaprakash AD, Tung N, Israelow B, et al. High-throughput assessment of microRNA activity and function using microRNA sensor and decoy libraries. Nat Methods 2012; 9:840-6; PMID:22751203; http://dx.doi.org/10.1038/nmeth.2078.
43. Schulz A, Toedt G, Zenz T, Stilgenbauer S, Lichter P, Seiffert M. Inflammatory cytokines and signaling pathways are associated with survival of primary chronic lymphocytic leukemia cells in vitro: a dominant role of CCL2. Haematologica 2011; 96:408-16; PMID:21134984; http://dx.doi.org/10.3324/haematol.2010.031377.
44. Dyer BW, Ferrer FA, Klinedinst DK, Rodriguez R. A noncommercial dual luciferase enzyme assay system for reporter gene analysis. Anal Biochem 2000; 282:158-61; PMID:10860516; http://dx.doi.org/10.1006/abio.2000.4605.
45. Anders S, Huber W. Differential expression analysis for sequence count data. Genome Biol 2010; 11:R106; PMID:20979621; http://dx.doi.org/10.1186/gb-2010-11-10-r106.
46. Gottwein E, Mukherjee N, Sachse C, Frenzel C, Majoros WH, Chi JT, et al. A viral microRNA functions as an orthologue of cellular miR-155. Nature 2007; 450:1096-9; PMID:18075594; http://dx.doi.org/10.1038/nature05992.
47. Gibcus JH, Tan LP, Harms G, Schakel RN, de Jong D, Blokzijl T, et al. Hodgkin lymphoma cell lines are characterized by a specific miRNA expression profile. Neoplasia 2009; 11:167-76; PMID:19177201.